University of Nebraska - Lincoln
DigitalCommons@University of Nebraska - Lincoln

Mechanical & Materials Engineering Faculty Publications

Mechanical & Materials Engineering, Department of

1-1-2010

Force–frequency effect of thickness mode langasite resonators

Haifeng Zhang
University of Nebraska-Lincoln, haifeng.zhang@unt.edu

Joseph A. Turner
University of Nebraska-Lincoln, jaturner@unl.edu

Jiashi Yang
University of Nebraska-Lincoln, jyang1@unl.edu

John A. Kosinski
US Army RDECOM CERDEC, ATTN: AMSRD-CER-IW-DT, john.kosinski@us.army.mil

Follow this and additional works at: http://digitalcommons.unl.edu/mechengfacpub

Zhang, Haifeng; Turner, Joseph A.; Yang, Jiashi; and Kosinski, John A., "Force–frequency effect of thickness mode langasite resonators" (2010). *Mechanical & Materials Engineering Faculty Publications.* Paper 101.
http://digitalcommons.unl.edu/mechengfacpub/101

This Article is brought to you for free and open access by the Mechanical & Materials Engineering, Department of at DigitalCommons@University of Nebraska - Lincoln. It has been accepted for inclusion in Mechanical & Materials Engineering Faculty Publications by an authorized administrator of DigitalCommons@University of Nebraska - Lincoln.

Ultrasonics 50 (2010) 479–490

Contents lists available at ScienceDirect

Ultrasonics

journal homepage: www.elsevier.com/locate/ultras

Force–frequency effect of thickness mode langasite resonators

Haifeng Zhang [a,1], Joseph A. Turner [a,*], Jiashi Yang [a], John A. Kosinski [b]

[a] Department of Engineering Mechanics, University of Nebraska-Lincoln, W317.4 Nebraska Hall, Lincoln, NE 68588, United States
[b] US Army RDECOM CERDEC, ATTN: AMSRD-CER-IW-DT, Fort Monmouth, NJ 07703-5211, United States

ARTICLE INFO

Article history:
Received 9 April 2009
Received in revised form 9 October 2009
Accepted 9 October 2009
Available online 29 October 2009

Keywords:
Force–frequency effect
Langasite
Resonators

ABSTRACT

Langasite resonators are of recent interest for a variety of applications because of their good temperature behavior, good piezoelectric coupling, low acoustic loss and high Q factor. The force–frequency effect describes the shift in resonant frequency a resonator experiences due to the application of a mechanical load. A clear understanding of this effect is essential for many design applications such as pressure sensors. In this article, the frequency shift is analyzed theoretically and numerically for thin, circular langasite plates subjected to a pair of diametrical forces. In addition, the sensitivity of the force–frequency effect is analyzed with respect to the nonlinear material constants. The results are anticipated to be valuable for experimental measurements of nonlinear material constants as well as for device design.

© 2009 Published by Elsevier B.V.

1. Introduction

Piezoelectric resonators based on langasite and its isomorphs [1–3] are of current interest in the piezoelectric device community based on the combination of moderately strong piezoelectric coupling, low acoustic loss, zero temperature coefficient of frequency, and reduced nonlinear effects occurring in simple orientations. One of these nonlinear effects is the force–frequency effect which describes the resonant frequency shift that occurs when the resonator is subjected to an external mechanical load (here, an applied diametrically oriented force pair). Depending upon the design of the resonator mounting structure, this effect can cause problems with resonators used in timing devices when external accelerations are experienced. One approach to counteract the frequency shift caused by acceleration is to actively adjust the frequency with another nonlinear effect, namely the electroelastic effect [4–6]. Alternatively, the force–frequency effect can also be used to produce a force sensor [7,8]. The first examination of the force–frequency effect in langasite was published by Boy et al. in 2001 [9]. Their work on langasite included both theoretical and experimental components, drawing significant attention to the "major discrepancy" found for the magnitude of the effect in langasite. The experimental measurements of Boy et al. also included langatate (LGT), subsequently measured by Kim and Ballato along with langanite (LGN) [10]. Neither work included calculations for LGT or LGN as the required nonlinear material constants have not been measured. Independent calculations on the force–frequency effect in langasite were reported in [11] based upon an assumed isotropic biasing stress. The isotropic stress assumption was consistent with previous analyses of quartz resonators [12] and the results for quartz were shown to be consistent with the earlier work. The implication was that the results for langasite are a similarly good approximation. Unfortunately, these prior analyses ignored the influence of linear and nonlinear piezoelectric constants. For langasite single crystals which have moderately high piezoelectric coupling, those assumptions may be invalid. Consequently, in this article we improve the calculations of the force–frequency effect in langasite resonators by taking into account the full set of material nonlinearities and by determining more accurately the biasing stress and strain fields. The complete set of linear and nonlinear material constants may be necessary for estimations of the force–frequency effect for langasite resonators.

The force–frequency effect is caused by intrinsic nonlinear material properties of the single crystal. The nonlinear material properties are characterized by the third-order material constants including the third-order elastic, piezoelectric, dielectric and electrostrictive constants. A detailed description of this phenomenon requires the theory of infinitesimal fields superposed on finite biasing fields [13], which describes the influence of a biasing effect (mechanical stress, electrical field) on the natural frequency of piezoelectric resonators. For most (but not all) cases of interest, the

* Corresponding author.
E-mail address: jaturner@unl.edu (J.A. Turner).
[1] Present address: Department of Engineering Technology, University of North Texas, Denton, TX 76207, United States.

0041-624X/$ - see front matter © 2009 Published by Elsevier B.V.
doi:10.1016/j.ultras.2009.10.008

This article is a U.S. government work, and is not subject to copyright in the United States.

shifted value of the natural frequency can be estimated by the first-order perturbation integral [14].

To calculate the frequency shift of resonators subjected to a static mechanical load, one must first obtain the static solution for the strain and electrical field. However, because of the anisotropic material properties of the single crystal, it is difficult to obtain such solutions analytically. Previous research [9,11,12] has included several different approaches to both the isotropic and anisotropic solutions. The isotropic case provides a convenient initial estimate since the static solutions can easily be obtained in an analytical form that then enables a simple solution for the overall effect. Nevertheless, the true anisotropic solution differs sufficiently from the isotropic solution such that one must solve the fully anisotropic problem. An alternative method for this case is to use the finite element method (FEM). FEM is now commonly used in basic analyses of quartz resonators [15–19]. A previous FEM result for frequency shift estimates of quartz resonators can be found in [8] for which only the third-order elastic constants are considered. For quartz resonators with low piezoelectric coupling coefficient, this assumption may be accurate enough. However, it is unclear for langasite resonators with high piezoelectric coupling, whether other nonlinear material constants play an important role in this response. Given the difficulty of obtaining an analytical solution that includes all of the anisotropy and nonlinearity, in this article, FEM is used to estimate accurately the force–frequency effect of langasite resonators. The static anisotropic solution for a diametrical biasing stress is obtained using COMSOL. Combined with the analytical mode shape solutions, the force–frequency effect for a langasite resonator with arbitrary material orientations is obtained. All the third-order material constants including the third-order elastic, piezoelectric, dielectric and electrostrictive constants are used in the calculations. The results are compared both to an isotropic analytical solution and the limited experimental results reported in the literature. Finally, the influence from each group of nonlinear material constants is examined quantitatively by isolating the contributions of different sets of nonlinear material constants to the force–frequency effect for resonators with arbitrary material orientations. This sensitivity analysis is similar in objective but greatly expanded beyond that presented in Fig. 5 of [9] where the authors are simply attempting to explain the discrepancy in the magnitude of the theoretical and experimental results.

2. Perturbation integral

The resonant frequency of a resonator depends on its geometry, material constants and boundary conditions. When a langasite resonator is subjected to an external mechanical load, the geometry changes slightly. In this case, the material constants may be characterized as effective constants which will change with the external mechanical load. Thus, a resonant frequency will shift with the applied load. The shifted value may be estimated accurately by perturbation integral theory. The expression to estimate the first-order perturbation of a specific mode can be found from [14]

$$\begin{aligned}\Delta\omega_M &= \omega - \omega_M \\ &= \frac{1}{2\omega_M \int \rho_0 (u_1^M u_1^M + u_2^M u_2^M + u_3^M u_3^M) dV} \\ &\quad \times \int_V \left(\hat{c}_{K\alpha L\gamma} u_{\gamma,K}^M u_{\alpha,L}^M + 2\hat{e}_{KL\gamma} \phi_K^M u_{\gamma,L}^M - \hat{\varepsilon}_{KL} \phi_{,K}^M \phi_{,L}^M \right) dV, \end{aligned} \tag{1}$$

where

$$\hat{c}_{K\alpha L\gamma} = T_{KL}^0 \delta_{\alpha\gamma} + c_{K\alpha LN} w_{\gamma,N} + c_{KNL\gamma} w_{\alpha,N} + c_{K\alpha L\gamma AB} S_{AB}^0 + k_{AK\alpha L\gamma} E_A^0, \tag{2}$$

$$\hat{e}_{KL\gamma} = e_{KLM} w_{\gamma,M}^0 - k_{KL\gamma AB} S_{AB}^0 + b'_{AKL\gamma} E_A^0, \tag{3}$$

$$\hat{\varepsilon}_{KL} = b'_{KLAB} S_{AB}^0 + \chi_{KLA} E_A^0, \tag{4}$$

with

$$b'_{AKL\gamma} = b_{ABCD} + \varepsilon_0 \delta_{AB} \delta_{CD} - \varepsilon_0 (\delta_{AC} \delta_{BD} + \delta_{AD} \delta_{BC}).$$

In Eqs. (1)–(4), ω_M is the unperturbed angular frequency, ω is the perturbed angular frequency, and $\Delta\omega_M$ is the angular frequency shift. Here, $\hat{c}_{K\alpha L\gamma}$, $\hat{e}_{KL\gamma}$, and $\hat{\varepsilon}_{KL}$ are the effective elastic, piezoelectric, and dielectric constants respectively; u_γ^M is a specific mode shape function in the unperturbed condition and ϕ^M is the electrical potential for this specific mode. $T_{KL}^0, S_{AB}^0, E_A^0$ are the initial stress, strain and electrical field respectively with $w_{\gamma,N}$ defining the displacement gradient. $c_{K\alpha L\gamma}, d_{fAB}, \varepsilon_{KL}$ are the second-order elastic, piezoelectric and dielectric constants. $c_{K\alpha L\gamma AB}, k_{fK\alpha L\gamma}$, and χ_{KLf} are the third-order elastic, piezoelectric, and dielectric constants respectively and $b_{fAL\gamma}$ are the electrostrictive constants. ε_0 is the permittivity of free space. It is worth noting that the definition of the energy density used here differs from that of Sorokin [20]. The resulting differences in material constants are discussed in Appendix A.

The displacement gradient is the summation of strain and the rigid body rotation tensor. It may be written

$$w_{\gamma,N} = S_{\gamma N} + \Omega_{\gamma N}.$$

Physically, it can be easily verified that a rotation of the position of a crystal resonator will not cause a resonant frequency shift. More precisely, it has been proven in [21] that an arbitrary pure homogeneous infinitesimal rigid body rotation has no influence on frequency shift. Thus, in the case considered here, the displacement gradient may be obtained directly from the static strain solution.

The frequency shift, as given by Eq. (1), is a function of the mode, the natural frequency without perturbation, and the effective material constants. From Eqs. (2)–(4), the effective materials constants are functions of the initial stress and strain and the electrical field. Thus, estimates of the frequency shift of a resonator under an external mechanical load require the mode shape and stress as well as the strain and electrical field distribution for the resonator. In addition, the static solution for the electrical field, initial stress, and strain are required. In theory, these solutions may be obtained analytically or numerically and occasionally exact analytical solutions may be tractable.

For a resonator with simple geometry, the perturbation integral Eq. (1) may be simplified greatly. However, for a resonator with relatively complex geometry, the perturbation integral can be carried out only numerically. In such cases, the finite element solution combined with numerical integration may be used to estimate the resonator frequency shift. The initial stress, strain and field can be determined by finite element method for the element stress, strain and field. The volume integral can be treated as the summation of all element volumes. The perturbation integral for the finite element approach may then be expressed as

$$\Delta\omega_M = \Delta\omega_1 + \Delta\omega_2 - \Delta\omega_3, \tag{5}$$

where

$$\begin{aligned}\Delta\omega_1 = \sum_{N=1}^{ELN} &(T_{KL}^0(N)\delta_{\alpha\gamma} + 2c_{K\alpha LN} S_{\gamma N}^0(N) + c_{K\alpha L\gamma AB} S_{AB}^0(N) + k_{AK\alpha L\gamma} E_A^0(N) \\ &+ 2c_{K\alpha LN} \Omega_{\gamma N}^0(N)) u_{\gamma,K}^M(N) u_{\alpha,L}^M(N) V(N),\end{aligned}$$

$$\begin{aligned}\Delta\omega_2 = 2\sum_{N=1}^{ELN} &(e_{KLM}(S_{\gamma M}^0(N) + \Omega_{\gamma M}^0(N)) - k_{KL\gamma AB} S_{AB}^0(N) \\ &+ b'_{AKL\gamma} E_A^0(N)) \phi_K^M(N) u_{\gamma,L}^M(N) V(N),\end{aligned}$$

$$\Delta\omega_3 = \sum_{N=1}^{ELN} (b'_{KLAB} S_{AB}^0(N) + \chi_{KLA} E_A^0(N)) \phi_{,K}^M(N) \phi_{,L}^M(N) V(N).$$

Here, N is the element number and $T^0_{KL}(N)$, $S^0_{\gamma N}(N)$, $E^0_A(N)$, $V(N)$ are the element stress, strain, field and volume. If necessary, the rigid body rotation tensor $\Omega^0_{\gamma N}(N)$ can be calculated from the nodal displacements. The analytical solution to be derived in Section 3 is used for the mode shape $u_k(N)$ and field $\phi(N)$.

3. Unperturbed mode

Consider the free vibrations of a thin plate cut from a single crystal with arbitrary symmetry, as shown schematically in Fig. 1. The plate is fully coated with thin, massless electrodes on both sides. The boundary conditions are assumed traction free. Here, we approximate the exact mode as that for an infinite plate for simplicity. Later, we restrict our integration area to a region near the center of the plate in order to represent more closely the response expected from a trapped energy mode. Such an approximation is reasonable since errors in the mode shape result in high order behavior in the perturbation integral. In this case, the governing equations may be written

$$c_{2jk2}u_{k,22} + e_{22j}\phi_{,22} = \rho\ddot{u}_j, \tag{6}$$

$$e_{2k2}u_{k,22} - \varepsilon_{22}\phi_{,22} = 0. \tag{7}$$

The boundary conditions are written

$$T_{2j} = c_{2jk2}u_{k,2} + e_{22j}\phi_{,2} = 0, \tag{8}$$

$$\phi = 0, \quad \text{at } x_2 = \pm h. \tag{9}$$

The general solution for this case can be summarized as

$$u_j(x_2,t) = \sum_{i=1}^{3} D^i_j \sin\lambda_i x_2 e^{-i\omega t} = \sum_{i=1}^{3} K^i B^i_j \sin\lambda_i x_2 e^{-i\omega t}, \quad j = 1,2,3, \tag{10}$$

$$\phi(x_2,t) = \sum_{i=1}^{3}\left(K^i \frac{e_{11m}}{\varepsilon_{11}} B^i_m \sin\lambda_i x_2 + P_1 x_2 + P_2\right)e^{-i\omega t}, \quad m = 1,2,3, \tag{11}$$

where

$$P_1 = -\frac{1}{h}\sum_{i=1}^{3} K^i \frac{e_{11m}}{\varepsilon_{11}} B^i_m \sin\lambda_i h, \tag{12}$$

$$P_2 = 0. \tag{13}$$

Thus, the ith mode shape may be defined as

$$u^i_j(x_2) = D^i_j \sin\lambda_i x_2. \tag{14}$$

The amplitudes D^i_j are obtained by solving the eigenvalue problem

$$(c'_{2jk2} - c\delta_{jk})D_k = 0,$$

where

$$c'_{2jk2} = c_{2jk2} + (e_{22j}e_{22k})/\varepsilon_{22}.$$

Here, $(u^i_j(x_2))^M = B^i_j \sin\lambda_i x_2$ is the ith normalized mode shape and K^i is the normalized weighting coefficient, $\lambda_i = \sqrt{\rho\omega^2/c_i}$, with ω as the angular frequency. Substituting Eqs. (10) and (11) into boundary conditions, Eqs. (8) and (9), gives the transcendental equation which is used to determine the resonant frequencies. This equation is

$$\mathrm{Det}\left\{B^i_m[c'_{2jk2}\omega h\sqrt{c_i/\rho}\cos(\omega h\sqrt{c_i/\rho}) - (e_{22j}e_{22m}/\varepsilon_{22})\sin\omega h\sqrt{c_i/\rho}]\right\} = 0. \tag{15}$$

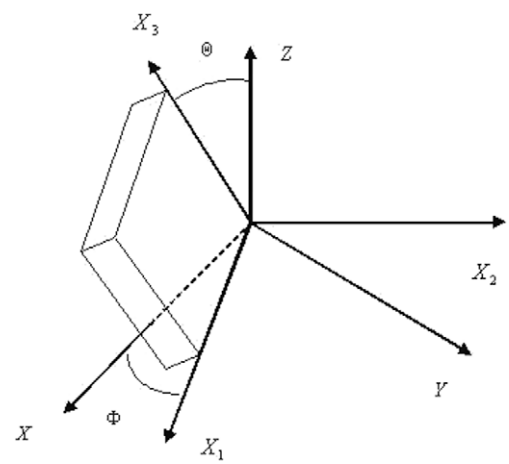

Fig. 2. Material orientation of a doubly rotated langasite resonator.

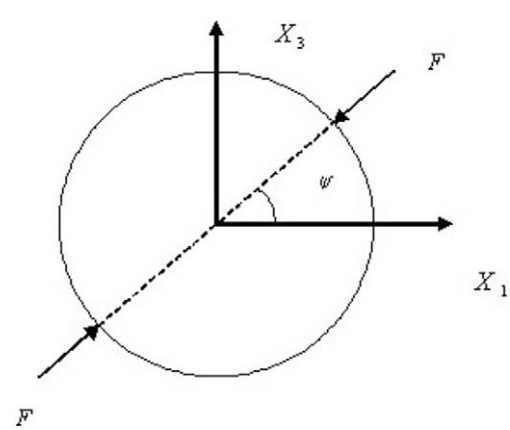

Fig. 3. The sketch of integration radius.

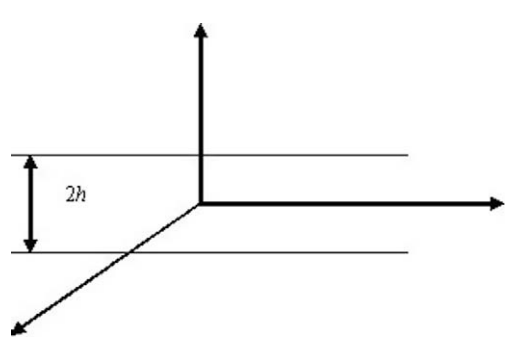

Fig. 1. A doubly-rotated langasite plate with electrodes on both sides.

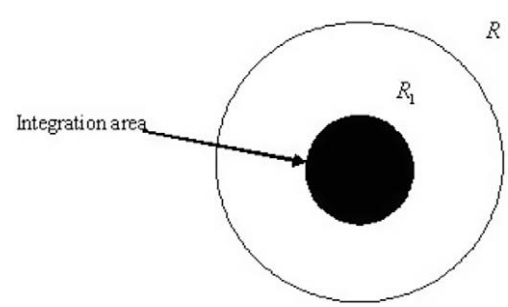

Fig. 4. A pair of diametric forces applied to the LGS resonator.

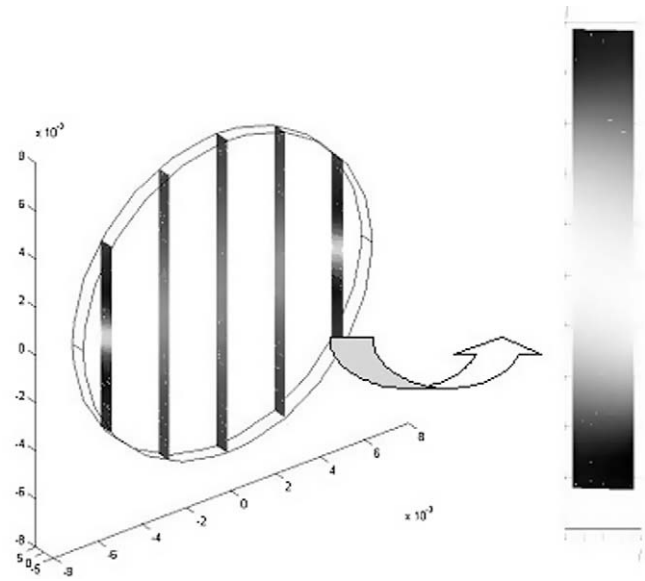

Fig. 5. Static solution for shear stress T_{12} determined by finite element method.

Eq. (15) is solved numerically for the frequencies of interest. Alternatively, the resonant frequency can be approximated by the anti-resonant frequency as [22]

$$\omega \approx \omega_1 = \frac{(2q-1)}{4h}\sqrt{\frac{c_j}{\rho}}, \quad j = 1,2,3, \quad q = 1,2,3,\ldots \tag{16}$$

Eq. (16) is often an accurate approximation for any overtone for materials with low piezoelectric coupling coefficient. For materials with high piezoelectric coupling coefficient, the approximation is accurate for high overtones ($q \geqslant 4$) where the $(1/(2q-1))^2$ reduction in effective coupling as a function of increasing harmonic results in a low effective piezoelectric coupling coefficient. Langasite has moderately high piezoelectric coupling. Therefore, Eq. (16) is expected to give accurate results only for high overtones.

4. Diametric force

4.1. Analytical solution

Consider a doubly-rotated langasite plate fully coated with electrodes on both sides as shown in Fig. 1. The material orientation is

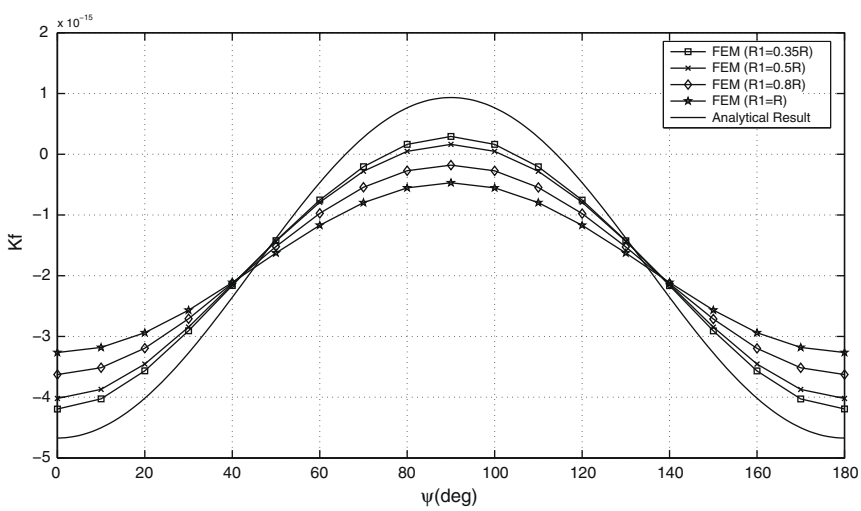

Fig. 6. The comparison between FEM result and theoretical result with different integral radius for the fast shear mode. The plot with mark is the FEM result with different integral radius, the line is the theoretical result.

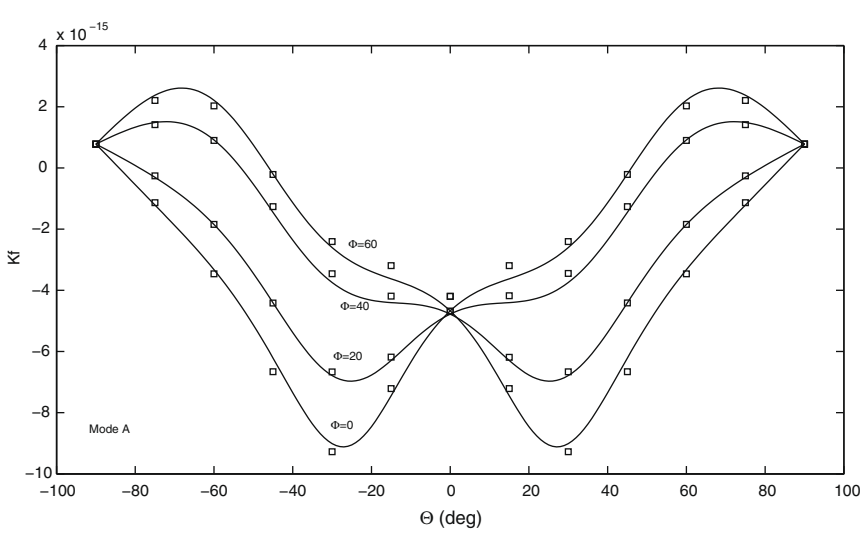

Fig. 7. The force–frequency effect of Y-cut thickness mode LGS resonators as a function of azimuth angle.

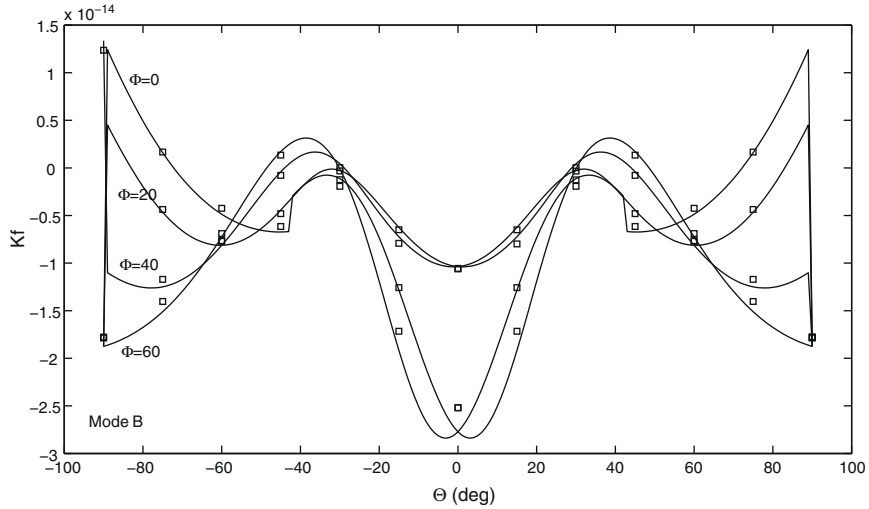

Fig. 8. Force–frequency effect of doubly rotated LGS resonator (YXwl $\Phi\Theta$) for mode A. The solid lines correspond to analytical solution, while the symbols denote the FEM solution.

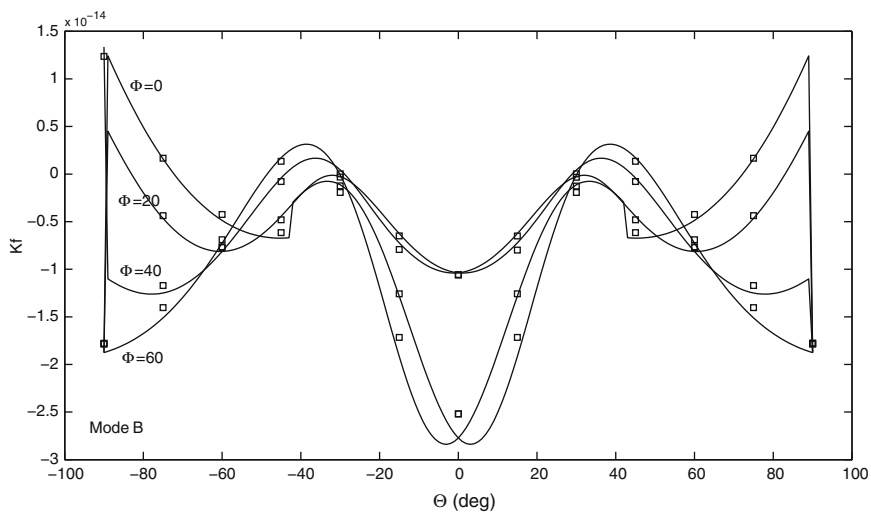

Fig. 9. Force–frequency effect of doubly rotated LGS resonator (YXwl $\Phi\Theta$) for mode B. The solid lines correspond to analytical solution, while the symbols denote the FEM solution.

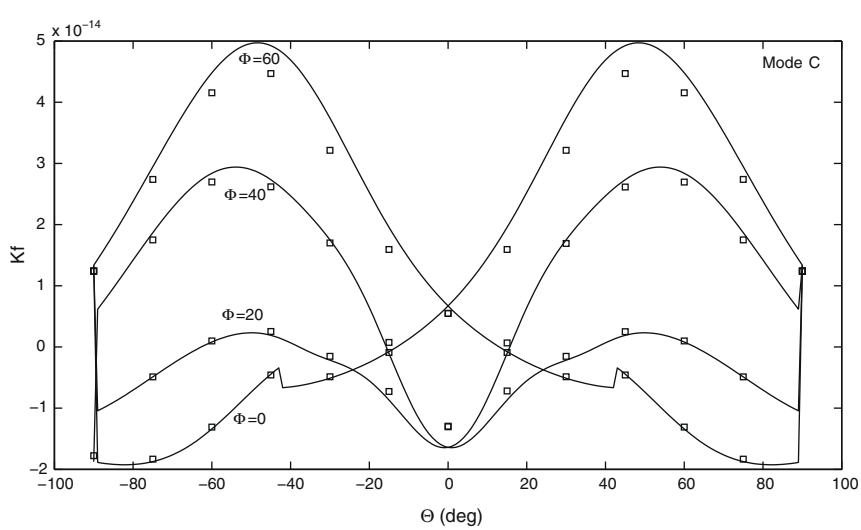

Fig. 10. Force–frequency effect of doubly rotated LGS resonator (YXwl $\Phi\Theta$) for mode C. The solid lines correspond to analytical solution, while the symbols denote the FEM solution.

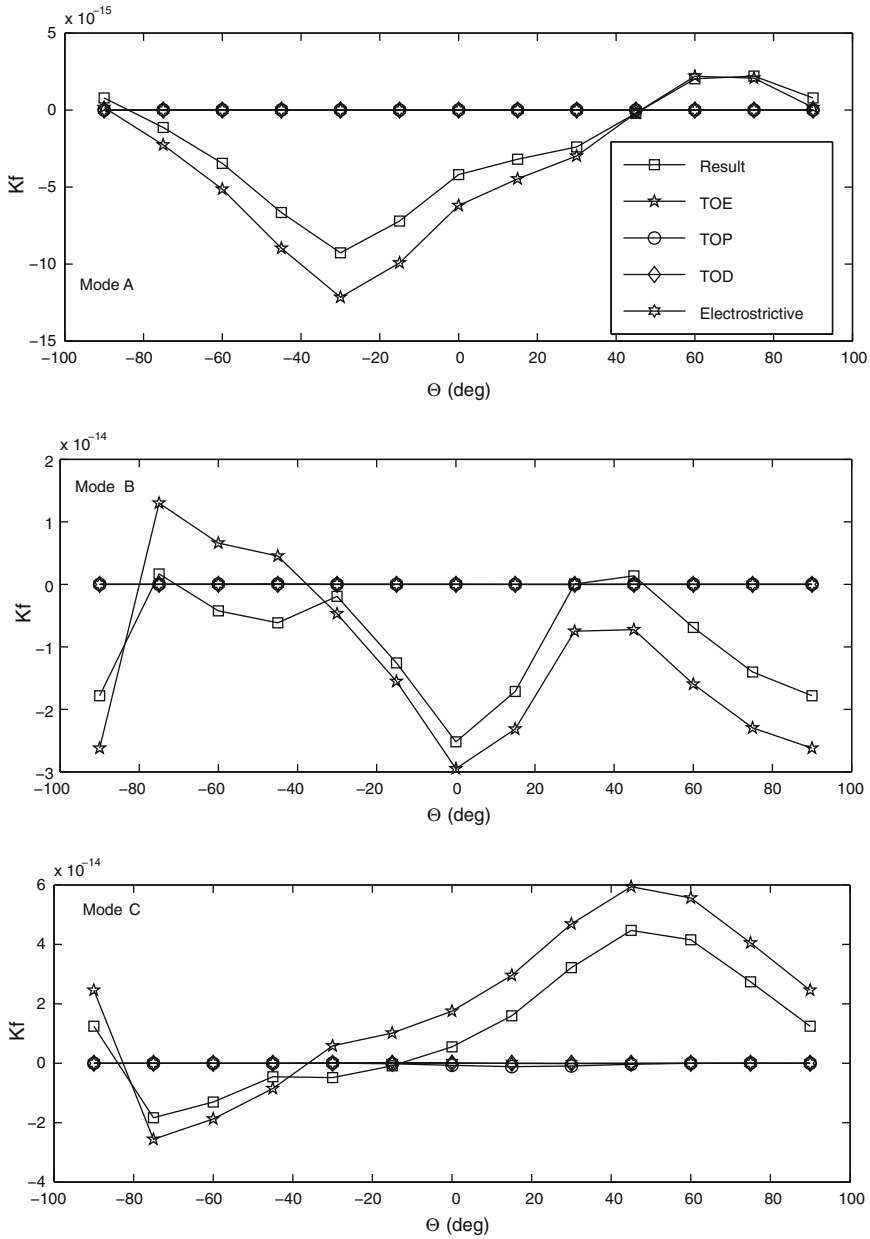

Fig. 11. The plots for the sensitivity of all group of nonlinear material constants to force–frequency effect ($\Phi = 0$). TOE (third-order elastic constants), TOP (third-order piezoelectric constants), TOD (third-order dielectric constants), ES (electrostrictive constants).

shown in Fig. 2 which follows IEEE standard 176–1987. A pair of equal forces F is applied in the diametric direction shown in Fig. 3. The three-dimensional linear equations of piezoelectricity can be written [23]

$$S_{ij} = s_{ijkl}T_{kl} - d_{kij}E_k, \tag{17}$$

$$D_i = d_{ikl}T_{kl} + \varepsilon_{ik}E_k, \tag{18}$$

$$T_{ji,j} = 0, \tag{19}$$

$$D_{i,i} = 0, \tag{20}$$

where the strain and the electric field are written

$$S_{kl} = (u_{k,l} + u_{l,k})/2, \tag{21}$$

$$E_k = -\phi_{7,k}. \tag{22}$$

As an approximation [12], the following stresses (at the center of an isotropic plate subjected to a pair of diametrical forces) are used throughout the thin plate

$$T_{11} = -\frac{6F}{\pi 2hD}, \quad T_{33} = \frac{2F}{\pi 2hD}, \quad T_{13} = 0. \tag{23}$$

Lee and Wu [24] used the uniform stress solution, Eq. (23), and then obtained the strain from an anisotropic constitutive model. They showed that such an approach matches force-frequency experiments well. Based on this approach, the stress distributions for the resonator subjected to a pair of diametrical forces are obtained as

$$T_{11} = -\frac{2}{\pi}\frac{F}{2hD}(1 + 2\cos 2\psi), \tag{24}$$

$$T_{33} = -\frac{2}{\pi}\frac{F}{2hD}(1 - 2\cos 2\psi), \tag{25}$$

$$T_{13} = -\frac{4}{\pi}\frac{F}{2hD}\sin 2\psi. \tag{26}$$

Then from the anisotropic strain and stress in Eq. (17), the strain components can be obtained.

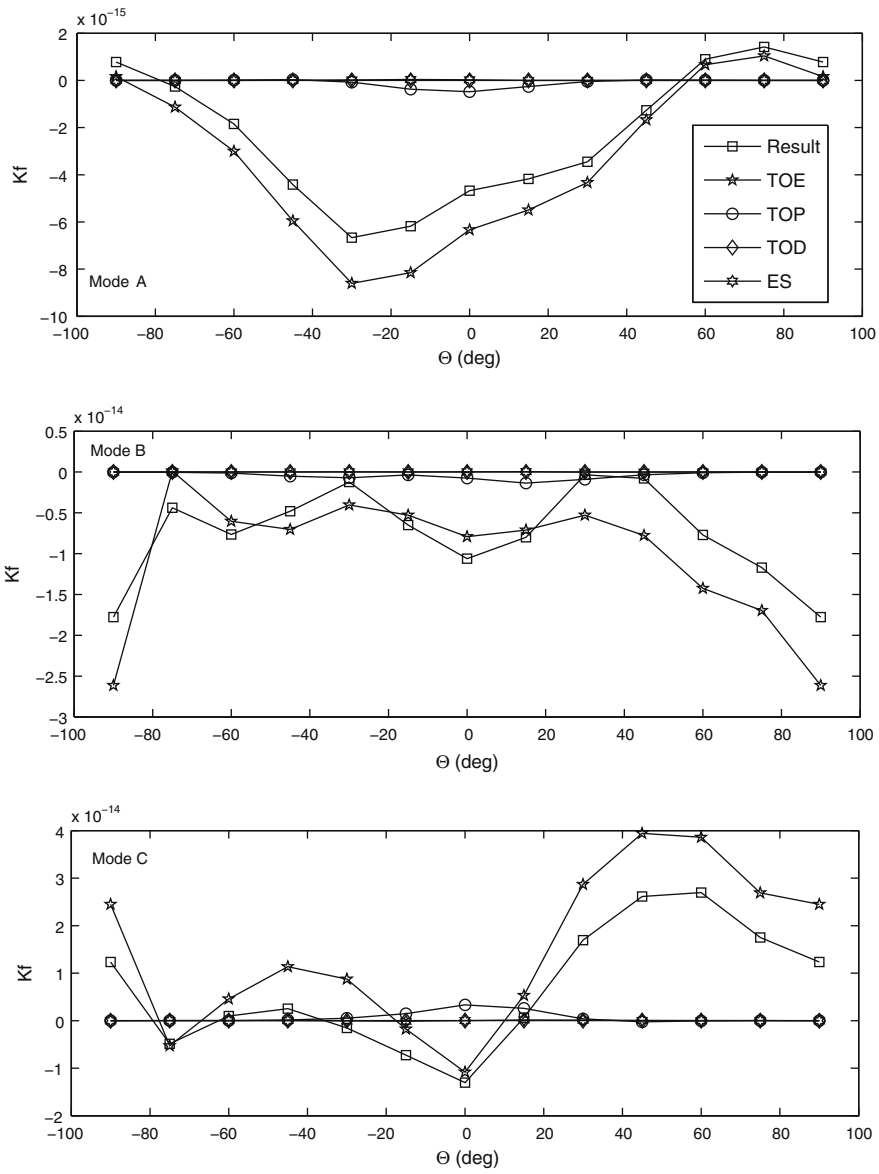

Fig. 12. The plots for the sensitivity of all group of nonlinear material constants to force–frequency effect ($\Phi = 20$). TOE (third-order elastic constants), TOP (third-order piezoelectric constants), TOD (third-order dielectric constants), ES (electrostrictive constants).

The force–frequency effect is often characterized by the force sensitivity coefficient which can be found in [25]. It is defined as

$$K_f(\phi,\theta,\psi) = \frac{\Delta f 2hD}{f_0 F f_0 (2h/n)} = \frac{\Delta f}{f_0}\frac{\text{Thickness}}{\text{Force}}\frac{\text{Diameter}}{(\text{Acoustic velocity})/2}, \tag{27}$$

where Δf is the natural frequency shift, h is the plate thickness, D is the plate diameter, f_0 is the unperturbed natural frequency, F is the diametric force, and n is the harmonic overtone order of the fundamental frequency. This coefficient is now examined for a variety of plate cuts.

4.2. Finite element solution

A finite element model for a doubly-rotated langasite resonator is constructed using FEMLAB 3.2 (COMSOL). The model includes 2224 Lagrangian quadratic elements with the number of boundary elements as 1640, such that there are three layers of elements. The sample radius is 6.5 mm, the thickness is 0.65 mm, and a pair of diametric forces is applied along the X axis. The radial edge of the plate has zero charge. The convergence of the numerical solution is verified by refining the element size and by comparison with analytical solutions when available. In the analytical approach, because of the isotropic material properties assumption, the stress distribution is uniform. The strain is then calculated by an anisotropic stress–strain constitutive equation, and the electrical charge and field are assumed zero. In the finite element approach, the plate is fully anisotropic and the influence of electrical charge and field are included in the analysis. Therefore, the FEM solution gives a more realistic result. Fig. 5 shows an example finite element solution for stress T_{12}. It can be seen that the solution is different from the isotropic solution, particularly away from the center of the plate, which illustrates a fundamental limitation of the isotropic assumption and the advantage of the FEM approach.

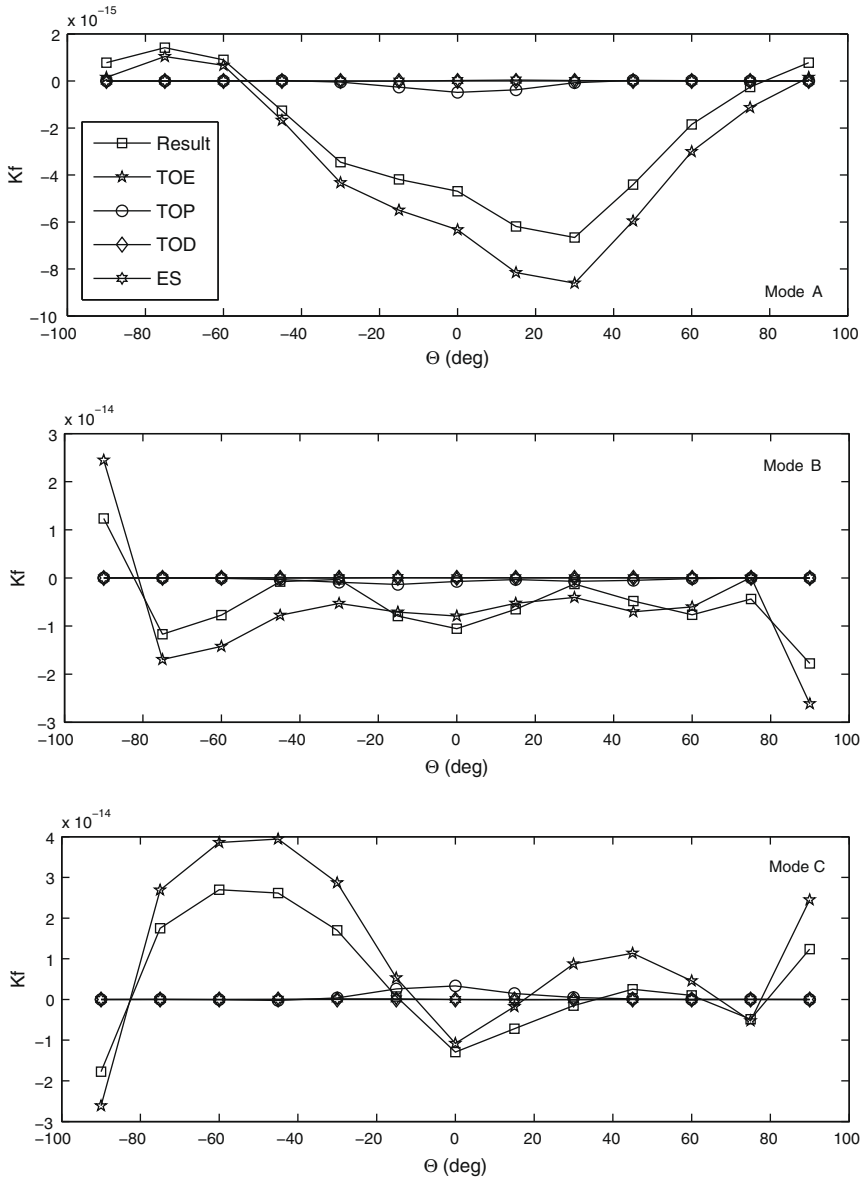

Fig. 13. The plots for the sensitivity of all group of nonlinear material constants to force–frequency effect ($\Phi = 40$). TOE (third-order elastic constants), TOP (third-order piezoelectric constants), TOD (third-order dielectric constants), ES (electrostrictive constants).

5. Results

For a resonator with arbitrary material orientation, the force–frequency effect for a specific mode is dependent on all material constants including second and third-order constants, after transforming them to the new coordinate. Secondly, the unperturbed natural frequency and mode shape for the specific mode are determined. Thirdly, the static stress, strain, and electrical field for the resonator under biasing diametrical forces are obtained. Finally, Eqs. (1) and (5), respectively, are used for the calculation of the force–frequency effect analytically and numerically. Example results are presented in this section, determined using the constants given in Tables A1–A8.

5.1. Force frequency effect

Figs. 6 and 7 shows the force–frequency effect of a Y-cut LGS resonator resulting from a pair of applied diametric forces. The approximate analytical results are obtained under the assumption that the thin plate is isotropic. Therefore, only the second-order and the third-order elastic constants are included in the perturbation integral calculations. FEM was also used to calculate the static strain solution for the anisotropic plate. All nonlinear material constants are included in the perturbation integral calculations. Fig. 6 also shows the results obtained using FEM to determine the influence of the integral volume with respect to the approximate analytical solution. Thus, R_1 defines the integral radius as a fraction of the plate radius. It is clear that the FEM results are closer to the approximate analytical result when the integral volume is restricted to the region near the center of the thin plate. This is because the FEM result assumes the analytical solution of the infinite plate, which may not apply near the edge of the plate. When the integration volume is restricted to the center region, the real mode shape is closer to the approximate analytical solution. Therefore, it appears that when R_1 (integral radius, shown in Fig. 4) = 0.35 R, the FEM result fits the analytical result well. Thus, this integration radius is used for the other results shown here. A more detailed analysis involving the exact trapped energy mode shapes is the subject of future work.

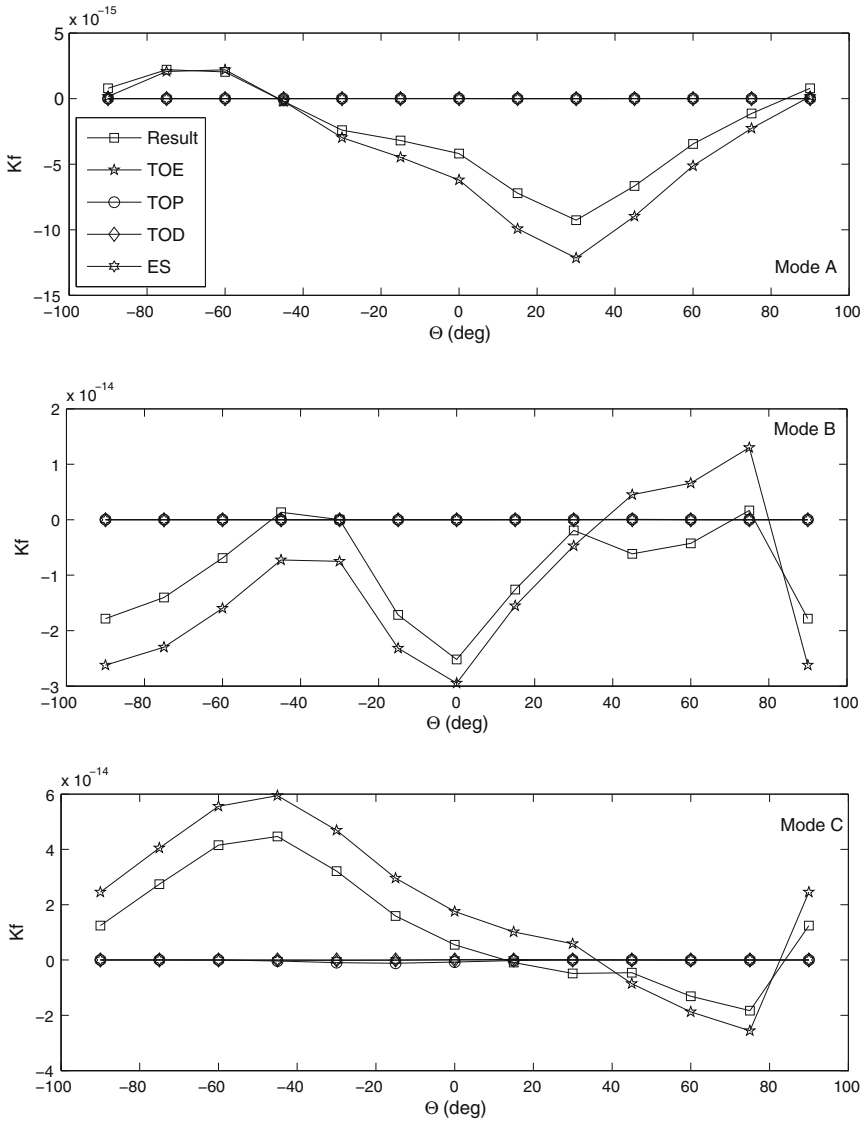

Fig. 14. The plots for the sensitivity of all group of nonlinear material constants to force–frequency effect ($\Phi = 60$). TOE (third-order elastic constants), TOP (third-order piezoelectric constants), TOD (third-order dielectric constants), ES (electrostrictive constants).

Figs. 8–10 show the force–frequency effect for the doubly-rotated LGS resonators (YXwl $\Phi, \Theta, \Phi = 0^\circ, 20^\circ, 40^\circ, 60^\circ$ with $\Theta = -90^\circ$ to 90°) when diametric forces are applied along the transformed X axis. Because the interest here is on the behavior with respect to the third-order material constants, only the contribution to the force–frequency effect from the third-order material constants is presented such that contributions from second-order material constants are excluded. The analytical results are shown as solid lines while the numerical results are denoted with squares. The FEM results and the approximate analytical results agree well for most cases, while there are certain orientations which have relatively large differences (e.g. the orientation: YXwl $\Phi = 60^\circ/\Theta = -90^\circ$ to 90°). For modes B and C, there are considerable jumps in the force–frequency effect at the cut YXwl $\Phi = 0^\circ,\ \Theta = \pm 43^\circ$. This result is due to a degeneracy that occurs at this cut. In this case, the first-order perturbation integral does not apply but the second-order perturbation integral [26] may be used. The intersections with the X axis indicate a possible stress compensation cut which can be used in the case which requires a minimum sensitivity to diametric forces.

5.2. Sensitivity to nonlinear material constants

As stated in Eq. (1), the natural frequency shift is related to all nonlinear material constants including the third-order elastic, piezoelectric, dielectric and electrostrictive constants. However, the contribution to the frequency shift from each group of nonlinear material constants depends on the cut angle. Therefore, to investigate the different contributions from different material constants quantitatively, we plot the contribution from each group of nonlinear material constants as a function of cut angle. Because nonlinear material constants are the major focus area in this article, the contribution of the second-order material constants is not shown in all sensitivity plots. Therefore, it is clear from the following figures that the total contribution from all nonlinear material constants does not match the complete curve, since it includes second-order effects as well.

Fig. 11 shows the force–frequency effect for cuts YXwl $\Phi = 0^\circ/\Theta = -90^\circ$ to 90°. The results for mode A (longitudinal mode) and B (fast shear) show that the primary contributions to the force–frequency effect come from the third-order elastic constants without any contribution from the third-order piezoelectric,

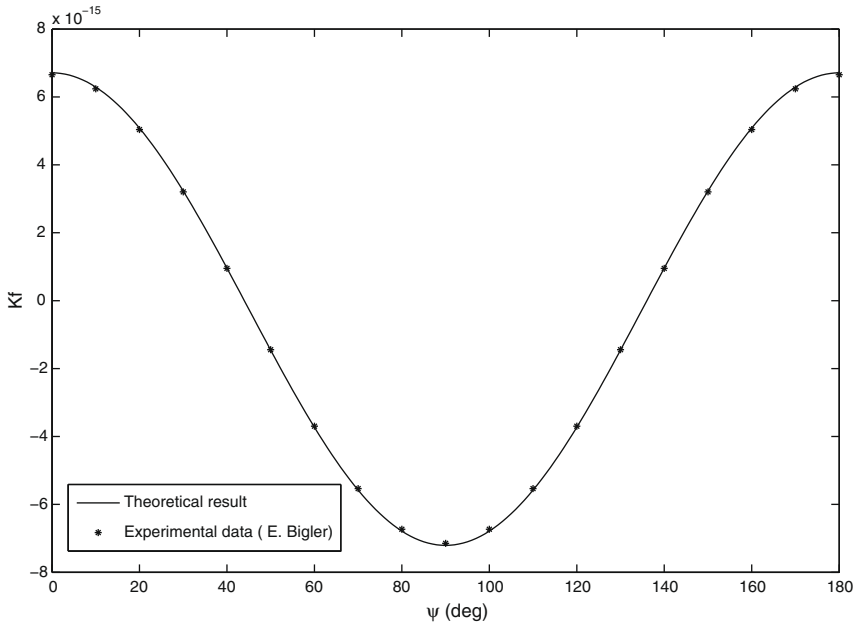

Fig. 15. The comparison of the theoretical result and the experimental data (J.J. Boy, E. Bigler) of a Y-cut 3rd overtone 9.98 MHz langasite resonator.

Table A1
A comparison between different material constant definitions.

Material constants	Ref. [20]	Here
2nd elastic	c_{ABCD}	c_{ABCD}
2nd piezoelectric	e_{ABC}	e_{ABC}
2nd dielectric	$\chi_{AB} + \varepsilon_0\delta_{AB}$	χ_{AB}
3rd elastic	c_{ABCDEF}	c_{ABCDEF}
3rd piezoelectric	$-k_{ABCDE}$	k_{ABCDE}
3rd dielectric	χ_{ABC}	χ_{ABC}
Electrostrictive	$b_{ABCD} + \varepsilon_0\delta_{AB}\delta_{CD} - \varepsilon_0(\delta_{AC}\delta_{BD} + \delta_{AD}\delta_{BC})$	b_{ABCD}

Table A2
Second-order elastic constants of langasite (10^{10} N/m^2).

c_{11}	18.875	c_{24}	1.412
c_{12}	10.475	c_{33}	2.614
c_{13}	9.589	c_{44}	5.35
c_{14}	−1.412	c_{55}	5.35
c_{22}	18.875	c_{56}	−1.412
c_{23}	9.589	c_{66}	4.2

Table A3
Second-order piezoelectrical constants of langasite (C/m^2).

e_{11}	−0.44	e_{21}	0	e_{31}	0
e_{12}	0.44	e_{22}	0	e_{32}	0
e_{13}	0	e_{23}	0	e_{33}	0
e_{14}	−0.08	e_{24}	0	e_{34}	0
e_{15}	0	e_{25}	0.08	e_{35}	0
e_{16}	0	e_{26}	0.44	e_{36}	0

Table A4
Second-order dielectric constants (10^{-12} C/V m).

ϵ_{11}	167.52
ϵ_{22}	167.52
ϵ_{33}	448.92

Table A5
Fourteen independent third-order elastic constants of langasite (10^{10} N/m^2).

c_{111}	−97.2	c_{134}	−4.1
c_{112}	0.7	c_{144}	−4.0
c_{113}	−11.6	c_{155}	−19.8
c_{114}	−2.2	c_{222}	−96.5
c_{123}	0.9	c_{333}	−183.4
c_{124}	−2.8	c_{344}	−38.9
c_{133}	−72.1	c_{444}	20.2

electrostrictive or the third-order dielectric constants. For mode C, it is observed that the cuts YXwl $\Phi = 0^\circ/\Theta = 0$–$30^\circ$ have small contributions from the third-order piezoelectric constants. Fig. 12 shows the results for cuts YXwl $\Phi = 20^\circ/\Theta = -90^\circ$ to 90°. Compared with the case shown in Fig. 11, we can see that except for the major contribution from the third-order elastic constants, the third-order piezoelectric constants play a more important role for a specific cut range (YXwl $\Phi = 0^\circ/\Theta = -30^\circ$ to 30° for mode A and C, YXwl $\Phi = 20^\circ/\Theta = -60^\circ$ to 45° for mode B). Therefore, if the third-order elastic constants of LGS are to be determined using an applied diametric load for LGS resonators, these cut ranges should be avoided. In Fig. 13, results are shown for mode C for the cut range YXwl $\Phi = 40^\circ/\Theta = -30^\circ$ to 30°, we notice that the influence of the third-order piezoelectric constants on the force–frequency effect is larger relative to other cut ranges. Therefore, this cut range may be good for determination of the third-order piezoelectric constants using an applied diametric load by resonator methods. In Fig. 14, we do not observe considerable contributions to force–frequency effect from the third-order piezoelectric constants for modes A and B. For mode C, the cut range YXwl $\Phi = 60^\circ/\Theta = -40^\circ$ to 0°, has little contribution from the third-order piezoelectric constants as well.

5.3. Comparison with previous experimental results

We compared our theoretical analysis result to the experimental result by Boy et al. [9]. The sample is a Y-cut 9.98 MHz 3rd overtone langasite resonator. The thickness is 0.41 mm, the external diameter is 13.2 mm and the electrodes are 6 mm, the radius of

Table A6
Eight independent third-order piezoelectrical constants of langasite (C/m^2).

e_{111}	9.3	c_{124}	−4.8
e_{113}	−3.5	e_{134}	6.9
e_{114}	1.0	e_{144}	−1.7
e_{122}	0.7	e_{315}	−4

Table A7
Third-order dielectric permeability (10^{-20} F/V).

χ_{111}	−0.5

Table A8
Third-order electrostrictive constants of langasite (10^{-11} N/V^2).

H_{11}	−26	H_{31}	−24
H_{12}	65	H_{33}	−40
H_{13}	20	H_{41}	−170
H_{14}	−43	H_{44}	−44

curvature is 500 mm. Fig. 15 shows the comparison of force–frequency effect for this langasite resonator. The approximate analytical results fit the experimental results very well. It is worth noting that approximate analytical calculation is restricted to a plano–plano resonator model.

6. Conclusions

In this article, the force–frequency effect and the related sensitivity analysis of thickness mode langasite resonator were examined both analytically and numerically. It was shown that the similarity of FEM results and theoretical results depends on integral volume. The integral region close to the center of the resonator gives closer agreement between the FEM and analytical result. In addition, possible stress compensation cuts were found and discussed. The sensitivity analysis shows that the electrostrictive constants and the third-order dielectric constants contribute little to the force–frequency effect for the majority of cuts examined. The major contributions to the force–frequency effect come from the third-order order elastic constants. The contribution from the third-order order piezoelectric constants is small in most cases. However, there do exist some cut ranges where the contributions from the third-order piezoelectric constants are large enough that they can not be ignored. Determination of the third-order elastic constants using an applied diametric load on a resonator is proven feasible for cut ranges where the contribution from the third-order elastic constants dominates. The comparison between our theoretical calculation result to previous experimental data for a Y-cut 3rd overtone langasite resonator shows good agreement.

Acknowledgments

E. Bigler is gratefully acknowledged for his assistance in providing the experimental data for inclusion in Fig. 15. We would also like to thank Bill Horton and Eric Hague of MtronPTI for their helpful suggestions for this article. [This research was supported by the Army Research Office under Grant No. DAAD19-01-1-0443.]

Appendix A

A.1. Energy density definition

The energy density is defined here as [13]

$$\rho_0\psi(S_{KL},E_K) = \frac{1}{2}c_{ABCD}S_{AB}S_{CD} - e_{ABC}E_AS_{BC} - \frac{1}{2}\chi_{AB}E_AE_B + \frac{1}{6}c_{ABCDEF}S_{AB}S_{CD}S_{EF} + \frac{1}{2}k_{ABCDE}E_AS_{BC}S_{DE} - \frac{1}{2}b_{ABCD}E_AE_BS_{CD} - \frac{1}{6}\chi_{ABC}E_AE_BE_C. \quad (28)$$

This energy density definition does not include the behavior relative to that in a vacuum. However, the energy definition given in [20] is the total electric enthalpy which includes the energy density in a vacuum. Thus, the definition of material constants differs from [20]. These constants must be modified before they can be used in the calculations presented. The responses obtained in both cases will then be identical. Table A1 lists the modifications needed. The complete set of material constants of langasite with respect to crystallographic axes X, Y, and Z are available in [20], and are listed in Tables A2–A8.

References

[1] H. Fritze, M. Schulz, H. Seh, H.L. Tuller, High temperature operation and stability of langasite resonators, Materials Research Society Symposium Proceedings 835 (2005) 157–162.
[2] N. Naumenko, Optimal cuts of langasite, $La_3Ga_5SiO_{14}$ for SAW devices, IEEE Transactions on Ultrasonics, Ferroelectrics, and Frequency Control 48 (2) (2001) 530–537.
[3] R.C. Smythe, Langasite, langanite, and langatate bulk-wave y-cut resonators, IEEE Transactions on Ultrasonics, Ferroelectrics and Frequency Control 47 (2) (2000) 355–360.
[4] V.J. Rosati, R.L. Filler, Reduction of the effects of vibration on sc-cut quartz crystal oscillators, in: Proceeding of 38th ASFC, 1981, pp. 117–121.
[5] V.J. Rosati, Suppression of vibration-induced phase noise in crystal oscillators: an update, in: 41st Annual Frequency Control Symposium, 1987, pp. 409–412.
[6] H. Zhang, J.A. Turner, J. Yang, J.A. Kosinski, Electroelastic effect of thickness mode langasite resonators, IEEE Transactions on Ultrasonics, Ferroelectrics, and Frequency Control 54 (10) (2007) 2120–2128.
[7] C. Barthod, New force sensor based on a double ended tuning fork, in: Proceeding of IEEE International Frequency Control Symposium, 2000, pp. 74–78.
[8] L.D. Clayton, E.P. Eernisse, Quartz resonator frequency shifts computed using the finite element method, International Journal for Numerical Methods in Engineering 36 (1993) 385–401.
[9] J.J. Boy, R.J. Besson, E. Bigler, R. Bourquin, B. Dulmet, Theoretical and experimental studies of the force–frequency effect in BAW LGS and LGT resonators, IEEE International Frequency Control Symposium and PDA Exhibition (2001) 223–226.
[10] Y. Kim, A. Ballato, Force–frequency effect of y-cut langanite and y-cut langatate, IEEE Transactions on Ultrasonics, Ferroelectrics, and Frequency Control 50 (2003) 1678–1682.
[11] J.A. Kosinski, R.A. Pastore, X. Yang, J. Yang, J.A. Turner, Stress-induced frequency shifts in langasite thickness-mode resonators, in: Proceedings of the Annual IEEE International Frequency Control Symposium, 2003, pp. 716–722.
[12] B.K. Sinha, Stress-induced frequency shifts in thickness-mode resonators, in: Proceedings of the IEEE Ultrasonics Symposium, 1980, pp. 813–818.
[13] J. Yang, An Introduction to the Theory of Piezoelectricity. Advances in Mechanics and Mathematics Band 9, Springer-Verlag GmbH, 2005.
[14] H. Tiersten, Perturbation theory for linear electroelastic equations for small fields superposed on a bias, Journal of the Acoustical Society of America 64 (1978) 832–837.
[15] C. Gehin, S. Samper, Y. Teisseyre, Mounting characterization of a piezoelectric resonator using FEM, in: Proceeding of IEEE International Frequency Control Symposium, 1997, pp. 630–633.
[16] D.R. Cowdrey, J.R. Willis, Finite element calculation relevant to AT-cut quartz resonators, in: Proceeding of IEEE International Frequency Control Symposium, 1973, pp. 7–10.
[17] Y.K. Yong, M.S. Patel, The impact of finite element analysis on the design of quartz resonators, in: Proceeding of IEEE International Frequency Control Symposium, 2006, pp. 9–23.
[18] M.S. Patel, Y.-K. Yong, M. Tanaka, T. Ima, Drive level dependency in quartz resonators, Proceeding of IEEE International Frequency Control (2005) 793–801.
[19] B. Dulmet, Finite element analysis of activity-dips in BAW resonators and sensors, in: Proceeding of IEEE International Frequency Control Symposium, 2002, pp. 179–190.
[20] B.P. Sorokin, P.P. Turchin, S.I. Burkov, D.A. Glushkov, K.S. Alexandrov, Influence of static electric field, mechanical pressure and temperature on the propagation of acoustic waves in $La_3Ga_5SiO_{14}$ piezoelectric single crystal, in: Proceeding of IEEE International Frequency Control Symposium, 1996, pp. 161–169.

[21] H.F. Tiersten, B.K. Sinha, Temperature dependence of the resonant frequency of electrode doubly rotated quartz thickness-mode resonators, Journal of the Acoustical Society of America 50 (1979) 8038–8051.
[22] IEEE Standard on Piezoelectricity, IEEE, New york, 1987.
[23] H.F. Tiersten, Linear Piezoelectric Plate Vibrations, Plenum, New York, 1969.
[24] P.C.Y. Lee, K.M. Wu, In-plane accelerations and forces on frequency changes in doubly-rotated quartz plates, Journal of the Acoustical Society of America 75 (1984) 1105–1117.
[25] J.M. Ratajski, Force–frequency coefficient of singly rotated vibrating quartz crystals, IBM Journal of Research and Development 12 (1968) 92–99.
[26] J.A. Kosinski, R.A. Pastore, J. Yang, X. Yang, J.A. Turner, Perturbation theory for degenerate acoustic eigenmodes, in: Proceedings of the 2003 IEEE International Frequency Control Symposium and PDA Exhibition Jointly with the 17th European Frequency and Time Forum, 2003, pp. 734–741.